Journal of Hazardous Materials 402 (2021) 123425

Contents lists available at ScienceDirect

Journal of Hazardous Materials

journal homepage: www.elsevier.com/locate/jhazmat

Ferrous iron enhances arsenic sorption and oxidation by non-stoichiometric magnetite and maghemite

Reto Gubler, Laurel K. ThomasArrigo*

Soil Chemistry Group, Institute of Biogeochemistry and Pollutant Dynamics, Department of Environmental Systems Science, ETH Zurich, Universitätstrasse 16, CHN, CH-8092 Zurich, Switzerland

GRAPHICAL ABSTRACT

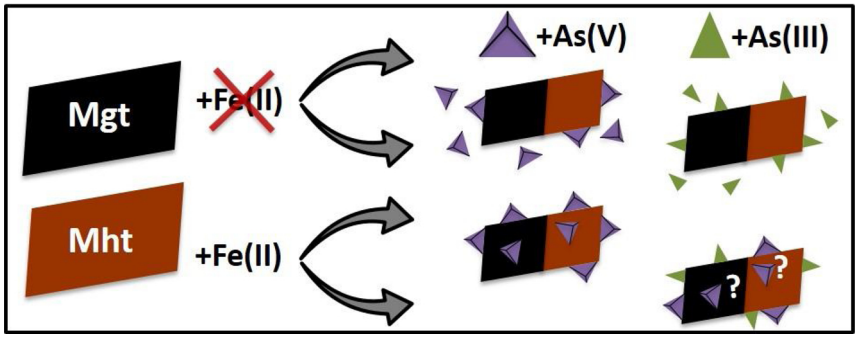

ARTICLE INFO

Editor: R Teresa

Keywords:
Redox cycling
Iron oxides
Fe(II)-catalyzed recrystallization
Arsenic
EXAFS spectroscopy

ABSTRACT

Arsenic-contaminated waters affect millions of people on a daily basis. Because the toxicity of As is dependent on the redox state, understanding As biogeochemistry, particularly in reducing environments, is critical to addressing the environmental risk that As poses. Sorption of As to Fe(III)-(oxyhydr)oxides is an important mechanism for As removal from solution under anoxic conditions. However, dissolved ferrous Fe (Fe(II)) also occurs under anoxic conditions, and the impact that Fe(II)-catalyzed recrystallization of crystalline Fe minerals has on As sorption mechanisms is not clear. Our research investigates the potential for non-stoichiometric magnetite, a commonly occurring mixed-valence Fe oxide in anoxic aquifers, to adsorb and/or incorporate inorganic As species during Fe(II)-catalyzed recrystallization at neutral pH, with particular focus on the impact of mineral stoichiometry (Fe(II):Fe(III) = 0.23 and 0.0) and varying Fe(II) concentrations. By following aqueous As concentrations and speciation over time coupled with As K-edge X-ray absorption spectroscopy, our results demonstrate that the presence of Fe(II) substantially enhanced As removal from solution. In addition, we highlight a Fe(II)-induced mechanism through which highly mobile, toxic As(III) species are oxidized on the mineral surface to form As(V). Furthermore, the presence of Fe(II) promotes the structural incorporation of As(V) into the non-stoichiometric magnetite and maghemite structures. These results highlight the potential of Fe(II)-reacted non-stoichiometric magnetite or maghemite as pathways for long-term As sequestration in anoxic environments.

* Corresponding author.
E-mail address: laurel.thomas@usys.ethz.ch (L.K. ThomasArrigo).

https://doi.org/10.1016/j.jhazmat.2020.123425
Received 15 April 2020; Received in revised form 3 July 2020; Accepted 5 July 2020
Available online 21 July 2020

1. Introduction

Elevated concentrations of As affect the daily lives of millions of people worldwide, many of whom rely on As-contaminated ground- and surface-waters for drinking and crop irrigation (Smedley and Kinniburgh, 2002). In natural waters at environmentally-relevant conditions (pH 3–9), As is primarily found as the inorganic species arsenate (As(V); $H_2AsO_4^-$ and $HAsO_4^{2-}$) and arsenite (As(III); $As(OH)_3$) (Smedley and Kinniburgh, 2002). Because the adsorption behavior of As changes with its redox speciation (Dixit and Hering, 2003), the mobility and toxicity of As are greatly dependent on As biogeochemistry. In soils and sediments, As redox chemistry is intimately linked to biogeochemical Fe cycling. Under oxic conditions, As is typically present as arsenate, which shows a high affinity for sorption to Fe(III)-(oxyhydr)oxides (Dixit and Hering, 2003). However, under reducing conditions, the microbially-mediated reduction of Fe(III)-(oxyhydr) oxides releases solid-phase associated As to solution (Burton et al., 2011, 2013; Cummings et al., 1999; Muehe et al., 2013), where As(V) may act as a terminal electron acceptor in microbial respiration (Jiang et al., 2013). Thus, arsenite often dominates under reducing conditions.

In the absence of oxygen, residual Fe(III)-(oxyhydr)oxides (Farquhar et al., 2002; Kocar et al., 2010; Muehe et al., 2013; ThomasArrigo et al., 2016) or secondary mineral phases (e.g. iron sulphides (Farquhar et al., 2002) or mixed-valence iron minerals (Jönsson and Sherman, 2008)) support the re-adsorption of dissolved As species. However, the microbially-mediated reduction of Fe(III)-(oxyhydr)oxides also leads to dissolved ferrous Fe (Fe(II)) in solution. In the presence of Fe(II), crystalline iron minerals (e.g. goethite; α-FeOOH, hematite; α-Fe_2O_3, magnetite; Fe_3O_4) undergo mineral recrystallization (Frierdich et al., 2015; Gorski et al., 2012; Handler et al., 2014); a process that has been shown to alter the distribution of mineral-associated trace metal(loid)s (e.g. Co, Cu, Mn, Ni, Sb, Zn,) (Burton et al., 2020; Frierdich and Catalano, 2012a, 2012) and, for some redox-sensitive species, lead to their reduction (Co, Cu, Mn) (Frierdich and Catalano, 2012a). However, the fate of redox-sensitive inorganic As species during Fe(II)-catalyzed mineral recrystallization is less understood. At relatively high Fe(II):Fe(III) molar ratios (0.5, 1, 2), Perez et al. recorded the reduction of As(V) during Fe(II)-catalyzed transformation of ferrihydrite into green-rust and goethite (Perez et al., 2019). In contrast, no changes in As species were reported during Fe(II) sorption to As(V)-associated goethite (Catalano et al., 2011), hematite (Catalano et al., 2011), or during the Fe(II)-catalyzed recrystallization of stoichiometric magnetite (Huhmann et al., 2017) under anoxic conditions. However, Amstaetter et al. reported that under dark, anoxic conditions, 'Fe(II)-activated' goethite (5.4 g goethite/L, 2.0 mM Fe(II)) oxidized 12 % of added As(III) (1.2 mg/L) after 7 days, suggesting the formation of a highly reactive surface precipitate as a plausible oxidation mechanism (Amstaetter et al., 2010). More recently, similar results have been reported for systems in which Fe(II) interactions with As(III)-bearing ferrihydrite ($Fe(OH)_3$) (Zhang et al., 2019), lepidocrocite (γ-FeOOH) (Wang and Giammar, 2015), and schwertmannite ($Fe_8O_8(OH)_{8-2x}(SO_4)_x$) (Burton et al., 2010) result in the oxidation of As(III) to As(V).

Because As(V) has a high sorption affinity (Dixit and Hering, 2003), the Fe(II)-catalyzed oxidation of As(III) to As(V) during mineral transformations or recrystallization has important implications for As mobility under reducing conditions. In anoxic aquifers, magnetite, a thermodynamically stable, mixed-valence Fe oxide, occurs naturally through both biogenic pathways (e.g. microbial Fe(II) oxidation (Chaudhuri et al., 2001) and dissimilatory Fe(III)-reduction (Lovley et al., 1987)) as well as abiotically; magnetite is an end product of Fe (II)-catalyzed transformations of ferrihydrite and lepidocrocite at pH ≥ 7 and at high $Fe(II):Fe(III)_{mineral}$ molar ratios (Aeppli et al., 2019; Hansel et al., 2003; Tamaura et al., 1983) and is often considered a potential candidate to remediate As-containing waters (Chowdhury et al., 2011; van Genuchten et al., 2020v). Under anoxic conditions, magnetite may coexist with Fe(II). To date, however, it is not known whether magnetite, like other iron minerals (Burton et al., 2010; Wang and Giammar, 2015; Zhang et al., 2019), can oxidize As(III) when coupled to Fe(II) sorption. Furthermore, recent research suggests that the As(V) tetrahedron may substitute for tetrahedral Fe(III) sites within the magnetite structure, thus leading to long-term As(V) immobilization. For example, Pedersen et al. reported decreases in desorbable As (V) fractions during the Fe(II)-catalyzed transformation of As(V)-adsorbed ferrihydrite and lepidocrocite into magnetite (Pedersen et al., 2006). Spectroscopic evidence of As(V) incorporation has been shown for magnetite formed via dissimilatory reduction of arsenic-bearing ferrihydrite (Coker et al., 2006), the Fe(II)-catalyzed transformation of As(V)-bearing lepidocrocite (Wang et al., 2014, 2011), Fe(0) electrolysis in the presence of As(V) (van Genuchten et al., 2020v), and aging batch studies comprising stoichiometric magnetite, As(V), and Fe(II) (Huhmann et al., 2017). In the latter, structural incorporation of As(V) occurred in both the presence and absence of Fe(II) with minimal net Fe (II) uptake and low (~10 %) atom exchange, thus leading the authors to suggest that the presence of Fe(II) was of minor importance (Huhmann et al., 2017).

However, stoichiometry controls the extent of Fe(II) uptake in magnetite, whereby Fe(II) uptake in stoichiometric magnetite is limited by a theoretical maximum bulk Fe(II)/Fe(III) ratio of 0.5 (Gorski and Scherer, 2009; Jolivet et al., 1992; Tronc et al., 1984). Moreover, magnetite stoichiometry has been shown to impact the mineral's capacity for reduction of trace metal(loid)s (Sundman et al., 2020), particularly in the presence of Fe(II) (Gorski and Scherer, 2009; Latta et al., 2012; Pasakarnis et al., 2013). Thus, it is plausible that Fe(II)-catalyzed recrystallization of As-associated non-stoichiometric magnetite may influence As distribution and speciation differently if it occurs concomitantly with Fe(II) uptake. Therefore, in this study, we followed the fate of As, initially present as As(V) or As(III), during Fe(II) interactions with non-stoichiometric magnetite (Fe(II)/Fe(III) = 0.23) and maghemite (Fe(II)/Fe(III) = 0.0) at neutral pH for one week. The extent of Fe (II) uptake and subsequent impact on mineral stoichiometry was determined with acid dissolution methods and X-ray diffraction, while time-resolved aqueous Fe and As speciation data revealed the impact of Fe(II) on As sorption kinetics. In addition, we utilized As K-edge X-ray absorption spectroscopy to determine solid-phase As speciation and assess the extent to which the presence and uptake of Fe(II) affected the local coordination environment of As at one week. The results present compelling evidence that the effectiveness of Fe(II)-activated magnetite as a pathway for long-term As sequestration in anoxic environments is highly dependent on magnetite stoichiometry.

2. Materials and methods

2.1. Solid-phase characterization

Synthetic magnetite (Mgt, nominal particle size 50 − 100 nm) was purchased from Alfa Aesar (97 %, metals basis) and stored in an anoxic glovebox (< 1 ppm O_2). Oxidized magnetite, or maghemite (Mht, γ-Fe_2O_3) was obtained by heating the synthetic magnetite for 2 h at 250 °C in a ceramic crucible in a combustion oven (Nabertherm). After heating, the black magnetite sample was brownish-red, consistent with maghemite (Fig. S1). Scorodite ($FeAsO_4{\cdot}2H_2O$) was synthesized as reported in Ehlert et al. (Ehlert et al., 2018). Mineralogy of the unreacted materials was confirmed using X-ray diffraction (XRD D8 Advance, Bruker). For these analyses, dried sample material (~5 mg) was resuspended in ethanol (~20 µL, Merck) and pipetted onto a polished silicon wafer (Sil'tronix Silicon Technologies, France). Samples were analyzed in Bragg-Brentano geometry using Cu Kα radiation (λ = 1.5418 Å, 40 kV, 40 mA) and a high-resolution energy-dispersive 1D detector (LYNXEYE). Diffractograms were recorded from 10 to 70 °2θ with a step size of 0.02°2θ and 6 s acquisition time per step. The relative contributions of mineral phases in diffraction patterns was determined

by Rietveld Quantitative Phase Analysis (QPA) in the TOPAS software (Version 5, Bruker AXS) using structure files for magnetite (Fleet, 1981), maghemite (Greaves, 1983), and scorodite (Xu et al., 2007). Total element contents of Mgt, Mht, and scorodite were determined with inductively coupled plasma-optical emission spectrometry (ICP-OES, Agilent 5100) after dissolution in concentrated HCl (Normatron®, VWR). For Mgt and Mht, Fe speciation (Fe(II) and Fe(total)) in the solid-phase was determined with UV–vis (Cary 60 UV–vis, Agilent) via the 1,10-phenanthroline method (Fortune and Mellon, 1938) after dissolution in 4 M HCl (target Fe concentration = 10 mM) (Gorski and Scherer, 2010) in a glovebox atmosphere. Magnetite nanoparticles dissolved within 5 h, while Mht nanoparticles required several days, in agreement slower acid dissolution rates expected for maghemite compared to magnetite (Sidhu et al., 1981). The electrophoretic mobility of the Fe solids was measured with a ZetaPALS Zeta Potential Analyzer (532-nm laser, Brookhaven Instr. Corp.). For these measurements, 250 mg/L of Mgt or Mht was re-suspended in 10 mM NaCl (EMSURE®, Merck). The solution was bubbled with N_2(g), while the pH was adjusted with dilute HCl or NaOH. Once the desired pH was obtained and remained constant for 10 min, the entire solution was ultrasonicated for 5 min. Then, an aliquot was removed and directly measured. The average electrophoretic mobility was determined from 10 runs comprising 10 cycles each. The measurements were repeated in duplicates, and the accuracy of the electrophoretic mobility measurement was checked against the BI-ZR3 zeta potential reference material (Brookhaven Instr. Corp.). The mineral specific surface area (SSA) of the solid-phases was determined by 11-point N_2-BET measurements (Quantachrome, Autosorb-1 MP) after 15 h of outgassing at 60 °C.

2.2. Arsenic sorption experiments

All solutions were prepared using doubly deionized water (DDI, Milli-Q®, Millipore, 18.2 MΩ cm. An Fe(II) stock solution of 100 mM was prepared by dissolving $FeCl_2{\cdot}4H_2O$ (VWR) in DDI water, and As(III) and As(V) stock solutions (2.67 mM) were prepared from $NaAsO_2$ (Fluka, > 99 %) and Na_2HAsO_4 (Sigma, > 98 %), respectively. All glassware was acid-washed and equilibrated in an anoxic glovebox (< 1 ppm O_2) for > 48 h. Experiments were completed in triplicate under glovebox atmosphere. In order to determine the impact that Fe(II)-Mgt/Mht interactions have on arsenic sorption, Mgt or Mht (1 g/L) was re-suspended in anoxic 50 mM 3-(N-morpholino)propanesulfonic acid buffer (MOPS, pH = 7) in Al-wrapped glass serum bottles with butyl rubber stoppers. After equilibrating overnight on an orbital shaker (200 rpm), aliquots of the Fe(II) stock solution were added to each reaction bottle to achieve $Fe(II)_{spike}$ concentrations of 0.1 or 1.0 mM. Bottles were allowed to react for 1 h, after which time aliquots of the As(III) or As(V) stock solution were added to obtain As concentrations of 2 mg/L (26.4 µM). Reaction bottles remained on the orbital shaker for up to 1 week, during which aliquots were removed for solid- and aqueous-phase sampling. The temperature and pH of the shaken solutions remained constant (23 ± 1 °C, pH = 7) for the duration of the experiment.

In order to determine whether surface Fe(II)-Mgt/Mht surface interactions were necessary to alter As sorption tendencies, a complimentary As sorption study was conducted with slight modifications to the experiment described above. These experiments were conducted at pH 5.5, where Fe(II) adsorption is limited (Handler et al., 2014; Reddy et al., 2015) and involved only Mgt and As(V). For these studies, 2-(N-morpholino)ethanesulfonic acid (MES) buffer was used. All other experimental parameters, including concentrations, analytical methods, and experimental duration, were retained.

2.3. Total aqueous Fe and As concentrations and speciation

Samples for aqueous analysis were collected at 1, 2, 4, 7, 25, 49, and 169 h after the Fe addition, with the addition of As taking place directly after the '1 h' sampling. Aqueous samples were filtered (0.22-µm nylon), and the filtrates measured for Fe(II) and Fe(total) with the 1,10-phenanthroline method (Fortune and Mellon, 1938) as described above. Aqueous As (As_{aq}) species in the filtrates were analyzed by hydride generation-atomic fluorescence spectrometry (HG-AFS, Millennium Excalibur, PS Analytical Ltd.) (Roberts et al., 2004). Solution concentrations of As(V) were inferred from the difference between As (total) and As(III) of the filtrates.

2.4. Reacted solid-phase sampling and speciation

Samples for solid-phase analyses were collected directly prior to the As addition (at 1 h) and after 1 week. Filter residues (0.45-µm filters) were washed with DDI water, covered and dried, manually homogenized, and stored in an anoxic glovebox until further analysis. Mineral stoichiometry was determined via XRD and UV–vis as described above, and total solid-phase Fe and As contents were determined with ICP-OES after dissolution in concentrated HCl.

To determine speciation changes of solid-phase As, Fe(II)-reacted Mgt and Mht were analyzed by bulk As K-edge (11,867 eV) X-ray absorption spectroscopy (XAS) at beamline 5-BM-D of the Advanced Photon Source (APS, Chicago, Il, USA). For these measurements, dried material was filled into Al sample holders and sealed with Kapton® tape. X-ray absorption near edge structure (XANES) and extended X-ray absorption fine structure (EXAFS) spectra were recorded in fluorescence mode with a 4-element Si-drift diode detector at ~80 K using a N_2(l) cooled spectroscopy stage (Linkam Scientific Instruments). The Si(111) monochromator was calibrated to the first-derivative maximum of the L3-edge absorption spectrum of a metallic Au foil (11,919 eV). Higher harmonics in the beam were eliminated by manually detuning the monochromator by 40 % of its maximal intensity. Four layers of Al foil were used to reduce undesired fluorescence and scattering contributions. For each sample, 4–8 scans were collected, dead-time corrected and averaged. All spectra were energy calibrated, pre-edge subtracted, and post-edge normalized in Athena (Ravel and Newville, 2005). The edge-energy, E_0, was defined as the highest peak in the first XANES derivatives. Linear combination fit (LCF) analyses of k^3-weighted As XANES spectra were conducted over an energy range of -20 to 30 eV (E-E_0) with E_0 of samples and reference compound spectra (As(V)- and As(III)-adsorbed to Mht at 7 days) defined as highest peak in their first XANES derivatives. No constraints were imposed on LCF fits, and initial fit fractions were recalculated to a compound sum of 100 %. Fourier transforms of k^3-weighted EXAFS spectra were calculated over a k-range of $2-12$ Å^{-1} using a Kaiser-Bessel window function with a sill width of 2.5 Å^{-1}. The frequency cut-off parameter, R_{bkg}, was set to 0.9. Shell-fit analyses of k^3-weighted As EXAFS spectra were performed in R-space (k-range = 2-11 Å^{-1}, R = 1–3.6 Å) using Artemis (Ravel and Newville, 2005). Theoretical phase-shift and amplitude functions were calculated with FEFF6 (Zabinsky et al., 1995) based on the structures of tooeleite (Morin et al., 2007) ($Fe_6(AsO_3)_4SO_4(OH)_4{\cdot}4H_2O$) and scorodite (Xu et al., 2007) ($FeAsO_4{\cdot}2H_2O$). The passive amplitude reduction factor, $S_0{}^2$, was first determined for the reference mineral scorodite during a fit in which coordination numbers (CN) were fixed to theoretical values (Xu et al., 2007), and then fixed to the determined value for the experimental samples.

3. Results and discussion

3.1. Stoichiometry and properties of magnetite and maghemite

The total Fe contents of Mgt and Mht were identical (68.4 wt. %). Similarly, measured SSA of the solid-phases were nearly identical (9.7 and 8.6 m^2/g for Mgt and Mht, respectively), as were the estimated points of zero charge (PZC) (Mgt_{pzc} ~ 7.6, Mht_{pzc} ~ 8.0, Fig. S1). This confirms starting solid phases were similar with regards to surface area and charge. X-ray diffraction patterns of Mgt and Mht are shown in Fig.

S2, and confirm the absence of other crystalline mineral phases. Additional peaks visible in the Mht sample (indicated with red arrows) are attributed to additional symmetry related to the ordering of vacancies in the Mht structure (Annersten and Hafner, 1973; Gorski and Scherer, 2010). The stoichiometry of nanometer-sized Mgt and Mht can be estimated from the unit-cell parameters determined during Rietveld fitting of XRD patterns (Gorski and Scherer, 2010), whereby a fitted unit-cell length (a) of 8.396–8.400 Å is indicative of stoichiometric magnetite (Cornell and Schwertmann, 2003; Gotić et al., 2009) (Fe(II)/Fe(III) = 0.5). Because the atomic size of an Fe(II) atom is larger than that of an Fe(III) atom, oxidation of stoichiometric magnetite results in slightly smaller unit-cell lengths which range from 8.33 to 8.34 Å in completely oxidized magnetite (Cornell and Schwertmann, 2003) (Fe(II)/Fe(III) = 0.0). Accordingly, the unit-cell lengths of unreacted Mgt and Mht were 8.387 and 8.350 Å, respectively (Table S1), suggesting the partial oxidation of Mgt and near-complete oxidation of Mht. Mineral stoichiometry was confirmed after anoxic dissolution in 4 M HCl, which determined Fe(II)/Fe(III) ratios for Mgt and Mht to be 0.23 and 0.0 (Table S2). Thus, both XRD and acid dissolution data suggested that, despite storing our purchased magnetite under anoxic conditions, some oxidation occurred prior to the experiment.

3.2. Iron adsorption onto magnetite and maghemite

Trends in aqueous Fe during reactions between Fe(II) and Mgt and Mht are shown in Fig. 1. Because dissolved Fe(III) accounted negligibly towards to the total aqueous Fe trends at all data points (Figs. S4 and S5), aqueous Fe is reported in terms of Fe(II). As explained in the experimental set-up, both Mgt and Mht were equilibrated with 0.1 or 1.0 mM Fe(II) for 1 h prior to the As addition. Therefore, measurements of aqueous Fe(II) taken at 1 h and directly prior to the As addition are representative of rapid Fe(II)-Mgt/Mht surface sorption interactions. Accordingly, Fe(II) concentrations in related reaction bottles at 1 h were similar; 740 ± 6 and 38 ± 3 μM for Mgt and 841 ± 6 and 58 ± 1 μM for Mht reacted with 1.0 and 0.1 mM Fe(II), respectively ($\bar{x} \pm \sigma$). The higher extent of rapid Fe(II) sorption onto Mgt compared to Mht may reflect the slight variations in their measured PZC (Fig. S1). In the absence of subsequent As additions, Fe(II) concentrations in control treatments continued to drop rapidly and approached the detection limit (1.7 μM) for the 0.1 mM Fe(II) addition as early as 7 h after the Fe(II) addition for both Mgt and Mht (Fig. 1A,C). For the 1.0 mM Fe(II) addition, Fe(II) sorption was similar onto both Mgt and Mht, with neither treatment reaching equilibrium at the end of the experiment (Fig. 1B,D). The similarly high rate of Fe(II) removal from both Mgt and Mht is further evidence of Mgt oxidation prior to the experiment: for non-stoichiometric magnetite, exposure to Fe(II) results in its structural incorporation (Gorski and Scherer, 2009), thereby increasing the bulk Fe(II) content towards a theoretical maximum Fe(II)/Fe(III) ratio of 0.5 (Gorski and Scherer, 2009; Jolivet et al., 1992; Tronc et al., 1984). Thus, Fe(II) uptake is highly dependent on magnetite stoichiometry and net Fe(II) uptake by stoichiometric magnetite is limited (Gorski et al., 2012; Gorski and Scherer, 2009). Following the addition of As(V) or As(III) (after '1 h'), Fe(II) concentrations continued to drop in all treatment bottles. However, further Fe(II) sorption was hindered in the presence of As, with up to 46 % and 30 % less Fe(II) removed from solution at 7 days with As(III) and As(V) additions, respectively (Fig. 1). Because Fe(II) complexation with As(V) is weak (Langmuir et al., 2006), this may suggest that Fe(II) competed with As species for surface adsorption sites (Catalano et al., 2011).

Overall Fe(II) to Mgt/Mht ratios were relatively low (0.1/1.0 mM Fe(II):g Mgt/Mht), thus adsorption and/or uptake of Fe(II) with the 0.1 mM Fe(II) treatments were not expected to noticeably impact the Mgt or Mht stoichiometry (Tables S1 and S2). For the 1.0 mM treatments, assuming all Fe(II) removed from solution in the As-free treatments (~0.8 mM, Fig. 1) was structurally incorporated, changes to the mineral stoichiometry would also be minimal; from 0.23 to ~0.31 and 0.00 to ~0.07 for Mgt and Mht, respectively. For the As_{spike} treatments, where the extent of Fe(II) removal was lower (~0.5 mM, Fig. 1), expected changes to mineral stoichiometry were even smaller: from 0.23 to ~0.29 and 0.00 to ~0.04 for Mgt and Mht, respectively. Such small changes to stoichiometry were likely not be detectible via XRD (Gorski et al., 2012). However, small increases in the Fe(II)/Fe(III) ratio determined via acid dissolution of the solid-phase are recorded (Table S2). Magnetite or maghemite were the only crystalline mineral phases identified with XRD both after equilibrating with Fe(II) for 1 h, as well as in all experimental samples after 7 days, thus excluding the precipitation of ferrous arsenate minerals (Fig. S3).

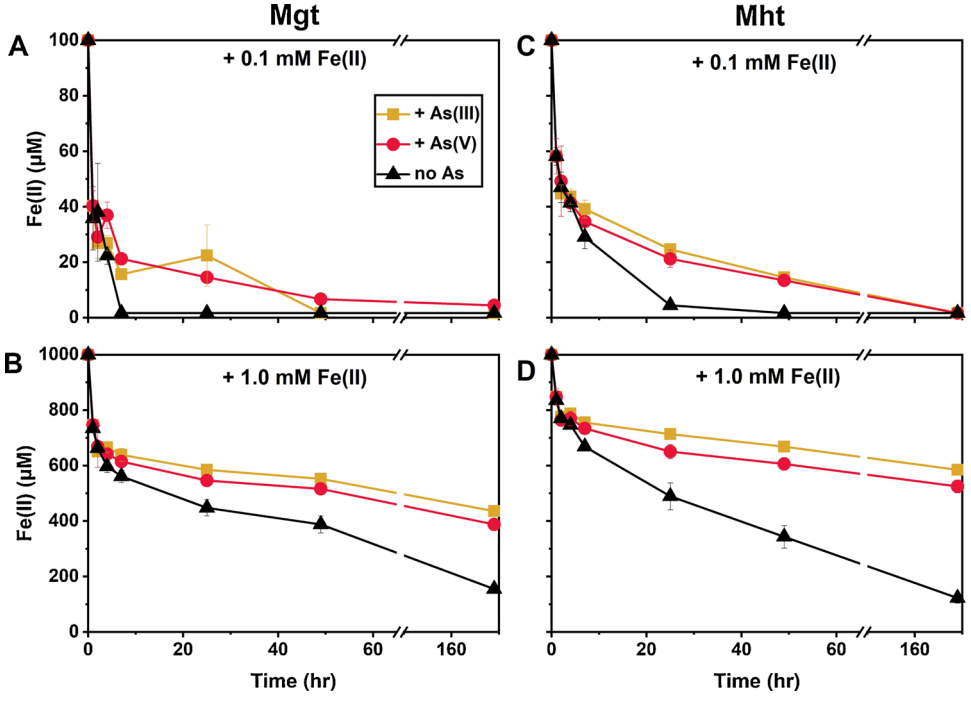

Fig. 1. Trends in dissolved Fe(II) determined in 0.22-μm filtrates for Mgt and Mht reacted with 0.1 or 1.0 mM Fe(II). Note that the solid-phases were equilibrated with 0.1 or 1.0 mM Fe(II) for 1 h prior to the addition of As(III) or As(V). Error bars represent the standard deviation from triplicate experiments. Please note the break in the x-axis.

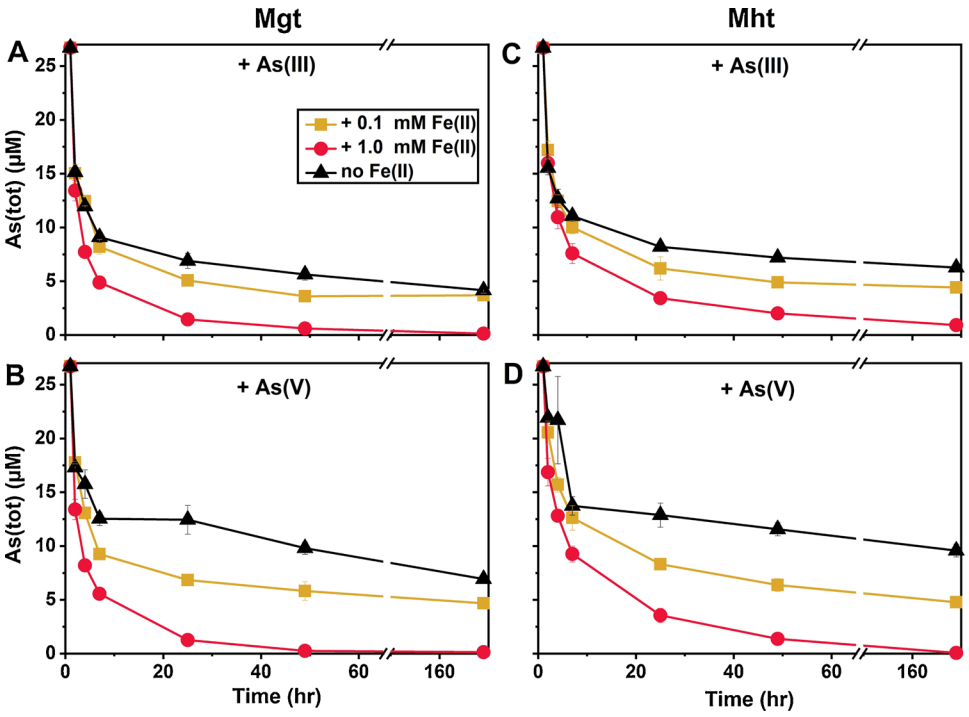

Fig. 2. Trends in total dissolved As determined in 0.22-µm filtrates for Mgt and Mht reacted with 0.1 or 1.0 mM Fe(II). Note that the solid-phases were equilibrated with Fe(II) for 1 h prior to the As addition, therefore trends in As begin at time = 1 h. Error bars represent the standard deviation from triplicate experiments. Please note the break in the x-axis.

3.3. Trends in arsenic sorption and speciation

Time-resolved trends in total aqueous As concentrations are shown in Fig. 2. In the absence of Fe(II), up to 84 % of added As was removed from solution within 1 week. At pH ≥ 8, As(III) is expected to sorb more strongly than As(V) to both magnetite and maghemite (Jönsson and Sherman, 2008; Morin et al., 2008; Yean et al., 2005). Here, we report similar results at pH 7, where As(III) sorbed more strongly than As(V) to both Mgt (+14 %) and Mht (+19 %). With the addition of 0.1 or 1.0 mM Fe(II), the differences between As(III) and As(V) sorption became negligible. However, a significant increase in overall As sorption was recorded in the presence of Fe(II); up to 21 % more As sorbed onto Mgt and Mht with the addition of 0.1 mM Fe(II). With the 1.0 mM Fe(II) addition, 15–36% more As sorbed, resulting in aqueous As concentrations near or below the drinking water limit of ~0.13 µM recommended by the World Health Organization (WHO, 2011) at 7 days (Fig. 2, Tables S4 and S5). For the negatively-charged As(V) species present at our experimental pH = 7 (H_2AsO_4– and $HAsO_4^{2-}$), this is in agreement with expected changes in Mgt/Mht surface potential towards positive values caused by Fe(II) sorption (Catalano et al., 2011). To prove this point, Fe(II)-Mgt-As(V) system sorption studies were repeated at pH 5.5, where Fe(II) adsorption is limited (Handler et al., 2014; Reddy et al., 2015), but As(V) sorption does not significantly differ (Liu et al., 2015). As Fig. S6 shows, at pH 7, 55–92 % of Fe(II) is removed from solution within 7 days, resulting in up to 26 % more As (V) sorption in the presence of 1.0 mM Fe(II). At pH 5.5, ≥96 % of Fe (II) remains in solution (Fig. S6). Correspondingly, differences in As(V) sorption between the Fe(II)-free and Fe(II)-addition treatments at pH 5.5 are reduced to < 8%, confirming that Fe(II) sorption is indeed necessary to promote enhanced As(V) sorption.

Increased As(III) sorption was also recorded in the presence of Fe (II). This may be explained through the formation of ternary complexes, as previously has been suggested for goethite-Fe(II)-As(III) systems (Dixit and Hering, 2006; Hiemstra and van Riemsdijk, 2007). The formation of such ternary complexes has been proposed to facilitate As(III) oxidation on Fe(II)-reacted goethite, whereby electron transfer between Fe(II) and the goethite surface results in a highly reactive Fe(III) phase potentially capable of As(III) oxidation (Amstaetter et al., 2010). Recent evidence of a highly reactive, labile Fe(III) phase formed during Fe(II) interactions with ferrihydrite supports this idea (Sheng et al., 2020). In agreement with As(III) oxidation on the mineral surface, analyses of As speciation in solution detected As(V) in both Mgt and Mht reacted with Fe(II) and As(III) as early as 1 h after the As(III) spike (Tables S4 and S5). Averaged over 1 week, contributions of As(V) to total As_{aq} were similar for both Mgt and Mht: $\bar{x}$ = 8 % and 15 % for 0.1 and 1.0 mM Fe (II) treatments, respectively, with As(III)/As(V) ratios remaining relatively stable for the duration of the experiment (Tables S4 and S5). Negligible As(V) was detected in the absence of Fe(II) ($\bar{x}$ = 2.5 % of As_{aq}), and testing of the As(III) stock solution confirmed its III + oxidation state. Therefore, As(V) detected in the $As(III)_{spike}$ treatments likely formed via oxidation of As(III) on the Fe(II)-reacted Mgt and Mht mineral surface. Arsenite was negligible in all $As(V)_{spike}$ treatments ($\bar{x}$ = 2.5 % of As_{aq}), indicating that As(V) was not reduced and released to solution.

At 7 days, however, As_{aq} only accounted for up to 36 % of total As in the system ($\bar{x}$ = 3.8 %). Therefore, we also employed bulk As XAS in order to follow solid-phase changes in As speciation. Arsenic K-edge XANES spectra of experimental samples and their corresponding LCF fits are shown in Fig. 3 and Fig. S7, and results from LCF analysis are detailed in Table S6. In the absence of Fe(II), As XANES spectra of Mgt and Mht reacted with As(V) or As(III) showed maximums at ca. 11,874 or 11,871 eV (for As(V)- and As(III)-reacted samples, respectively), with no difference visible between 1 h and 7 days of reaction time (Fig. S7). This suggests that no reduction or oxidation of As occurred upon sorption of As to Mgt or Mht in the Fe(II)-free systems, in agreement with previous studies (Huhmann et al., 2017; Morin et al., 2008; Wang et al., 2008, 2011). In contrast, with an addition of 0.1 or 1.0 mM Fe(II), 9–54 % of solid-phase As comprised As(V) after 7 days in the $As(III)_{spike}$ treatments (Fig. 3, Table S6). Increasing Fe(II) concentrations resulted in higher rates of As(III) oxidation (29 and 54 % vs. 9 and 16 % for Mht and Mgt reacted with 1.0 and 0.1 mM Fe(II), respectively). Mgt generally facilitated more As(III) oxidation compared to Mht. Because the extent of Fe(II) sorption onto Mgt was higher compared to Mht (Fig. 1), this may suggest that Fe(II) uptake is important to facilitating As(III) oxidation. No changes in solid-phase As speciation were recorded in $As(V)_{spike}$ treatments, suggesting that, in agreement with aqueous data, As

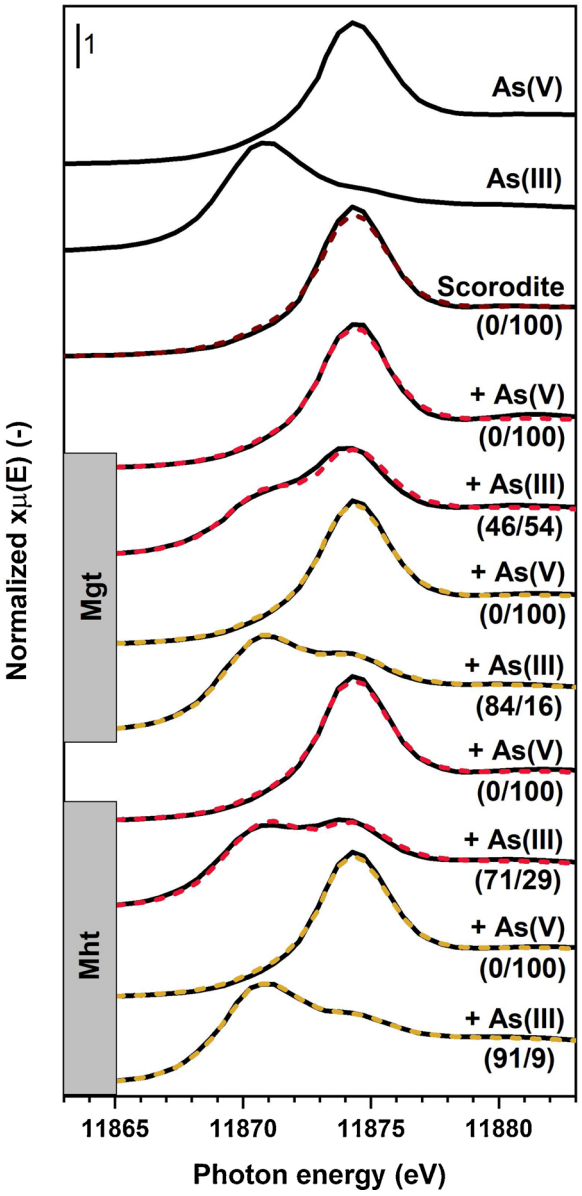

Fig. 3. Linear combination fits (LCF) of As K-edge XANES spectra of experimental samples and references. Experimental data and LCFs are shown in solid and dashed lines, respectively, for reactions with 1.0 mM Fe(II) additions (**red**) and 0.1 mM Fe(II) additions (**yellow**). Speciation of As spiked to the system is indicated above each data line. Arsenate and arsenite contributions determined during LCF analyses are shown in parentheses (As(III)/As(V), %). Details to LCF results are presented in Table S6. XANES spectra of control samples (As(III)- and As(V)-spiked samples in the absence of additonal Fe(II)) are shown in Fig. S7.

(V) was not reduced upon sorption to Fe(II)-reacted Mgt or Mht.

3.4. Coordination environment of solid-phase As

Arsenic K-edge EXAFS spectra and results of shell-fit analyses are illustrated in Figs. 4 and 5, and fit parameters are detailed in Table 1. All Fourier-transformed spectra showed a pronounced peak at $R+\Delta R \sim 1.3$ Å, arising from first-shell O atoms. For all $As(V)_{spike}$ samples, this feature was fit with an As-O path at a distance of 1.70 Å; in agreement with expected coordination within the AsO_4 tetrahedron (Xu et al., 2007). For $As(III)_{spike}$ samples, As-O fit distances varied from 1.79 Å in the Fe(II)-free controls to 1.73–1.78 Å in the Fe(II)-reacted systems. The longer distance (1.79 Å) is in agreement with expected coordination within the AsO_3 pyramid (Morin et al., 2007), while the shorter distances fit in the Fe(II)-reacted sample suggest a mixture of As (V) and As(III); in agreement with XANES LCF results (Fig. 3, Table S6).

Following the As-O shell, broad features are visible between $R+\Delta R$ = 2.3–3.3 Å; these result from multiple scattering (MS) paths within AsO_3 and AsO_4 polyhedra and distant Fe shells. For $As(V)_{spike}$ samples, the features between $R+\Delta R$ = 2.3–3.3 Å were successfully fit by a triangular As-O-O multiple-scattering (MS) path at ~3.09 Å, defined (non)collinear As-O-As-O MS paths (Catalano et al., 2011; Mikutta et al., 2010, Voegelin et al., 2007), and a single As-Fe path at 3.3–3.4 Å. Because substitution of the As(V) tetrahedron for tetrahedral FeO_4 within the magnetite or maghemite structure would result in two As-Fe paths at distances similar to the expected coordination environment of Fe(III) in tetrahedral magnetite sites (at 3.45 Å; *CN* = 12, and 3.61 Å; *CN* = 4) (Fleet, 1981; Greaves, 1983), the occurrence of a second As-Fe path at ~3.6 Å has been cited as evidence of As(V) incorporation into the magnetite structure (Coker et al., 2006; van Genuchten et al., 2020v; Wang et al., 2014, 2011). For our $As(V)_{spike}$ samples, although an additional As-Fe path at ~3.58 Å could be fit, this did not result in a statistically relevant improvement (Supplementary Material section 7) and was therefore not included in final fits. However, As-Fe path distances in the Fe(II)-reacted samples increased slightly compared to those in the Fe(II)-free controls at 7 days ($R_{As\text{-}Fe}$ = 3.39 Å vs. = 3.34 Å, ($\bar{x}$)). This may suggest that the local As coordination in the Fe(II)-reacted samples reflected a combination of monodentate binuclear (^{2}C) complexes (IUPAC, 2005) expected for surface adsorbed As(V) ($R_{As\text{-}Fe}$ = 3.33–3.36 Å) (Coker et al., 2006; Morin et al., 2008; van Genuchten et al., 2020v; Wang et al., 2011) and structurally incorporated As(V) ($R_{As\text{-}Fe}$ = 3.45 Å) (Coker et al., 2006; van Genuchten et al., 2020v; Wang et al., 2014, 2011). Slightly higher coordination numbers (*CN*) in the Fe(II)-reacted samples to the Fe(II)-free controls ($CN_{As\text{-}Fe}$ = 1.9 vs. = 1.4) indicates that the presence of Fe(II) resulted in increased As(V) sorption, in agreement with dissolved As data (Fig. 2).

For $As(III)_{spike}$ samples, the broad feature between $R+\Delta R$ = 2.3–3.3 Å was successfully fit with a triangular As-O-O MS path at ~3.18 Å and a single As-Fe path at 3.42–3.49 Å; both distances are slightly longer than those fit for $As(V)_{spike}$ samples (Fig. 5) and may represent a combination of ^{2}C complexes and monodentate mononuclear (^{1}V) complexes (Morin et al., 2008). Tridentate hexanuclear (^{3}C) complexes were not considered likely, as expected path distances for such complexes are longer ($R_{As\text{-}Fe}$ = 3.53 ± 0.02 Å) (Morin et al., 2009; Wang et al., 2008). Furthermore, the inclusion of an additional As-Fe path at ~2.90 Å, representative of bidentate mononuclear surface complexes (^{2}E) (Morin et al., 2008; Wang et al., 2008), did not result in a statistically relevant improvement (Supplementary Material section 7). Compared to the Fe(II)-free controls, *CN* for the As-Fe path in $As(III)_{spike}$ samples were higher, suggesting enhanced As(III) sorption in agreement with dissolved As data (Fig. 2). An exception is noted for Mgt reacted with 1 mM Fe(II), where smaller *CN* and path distance for the As-Fe shell are in agreement with a high fraction of solid-phase As(V) (54 %) contributing to shorter As-Fe paths. In general, results of shell-fit analyses for As in the Fe(II)-free controls matched the coordination environments expected for magnetite/maghemite adsorbed-As(V) and -As(III). In contrast, the presence of both 0.1 and 1.0 mM Fe(II) altered the extent of As sorption as well as impacted the local coordination of As, with differences slightly more noticeable with Mgt than for Mht (Table 1). This is particularly for As(V), where a shift towards longer As-Fe path distances suggested possible As(V) incorporation.

4. Conclusions

Collectively, our results show that As sorption to non-stoichiometric magnetite and maghemite under anoxic conditions is significantly increased in the presence of Fe(II), with more dramatic results obtained at higher Fe(II) concentrations. This may be partially explained through differences in the local coordination environment of As in Fe(II)-reacted

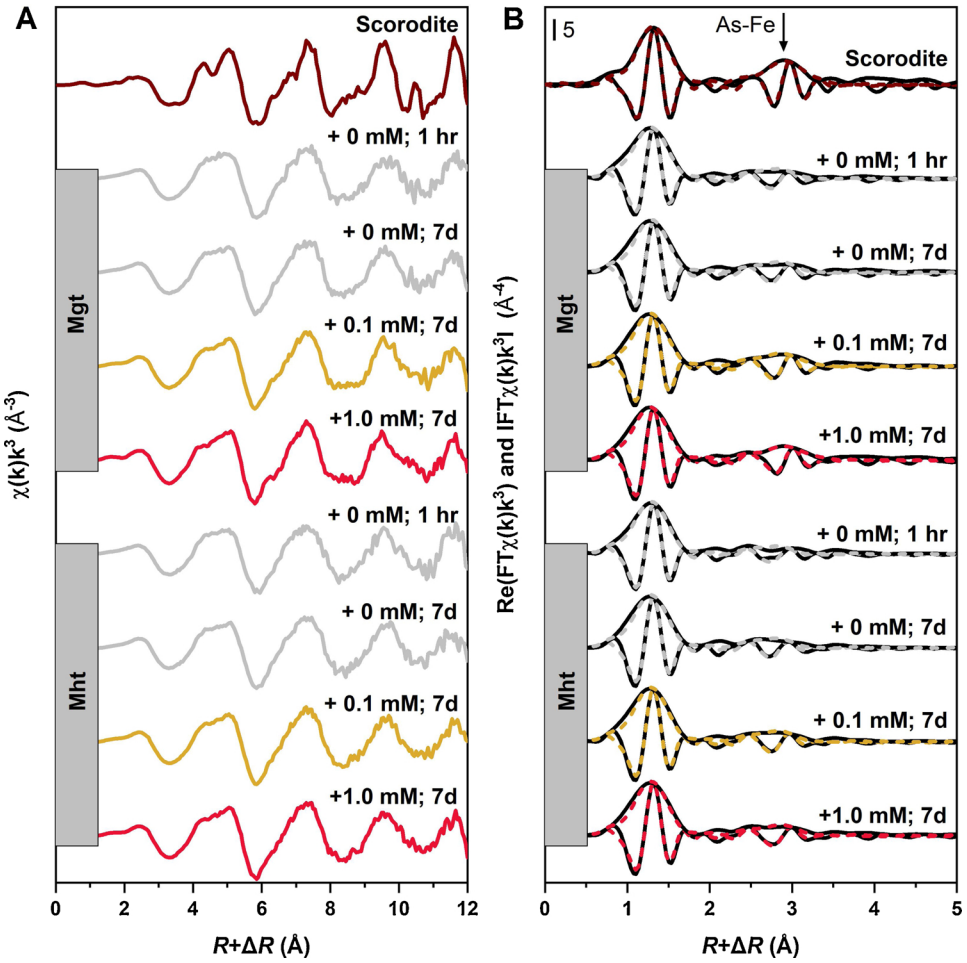

Fig. 4. (A) Arsenic K-edge EXAFS spectra and (B) Fourier-transform magnitudes and real parts shown for As(V)-spiked Mgt and Mht reacted with no additional Fe(II) (**gray**), 1.0 mM Fe(II) (**red**), and 0.1 mM Fe(II) (**yellow**). In (B), experimental data and model fits are shown in solid and dashed lines, respectively. Shell-fit parameters are reported in Table 1.

samples, which suggested the potential structural incorporation of As (V) into both Mgt and Mht. Furthermore, the presence of Fe(II) induced significant As(III) oxidation with both Mgt and Mht. The absence of O_2 in our system excludes As(III) oxidation by dissolved O_2, the kinetics of which could anyways not account for the rapid (< 1 h) appearance of As(V) in solution (Hug et al., 2001; Kim and Nriagu, 2000; Oscarson et al., 1980), and eliminates the explanation of rapid As(III) oxidation in systems comprising O_2 and Fe(II) (Hug et al., 2001; Hug and Leupin, 2003; Ona-Nguema et al., 2010) or O_2 and Fe(III)-(oxyhydr)oxides (Jang and Dempsey, 2008; Wang and Giammar, 2015). Similarly, photooxidation of As(III) during irradiation in the presence of Fe(III)-(oxyhydr)oxides (Bhandari et al., 2012, 2011; Hug et al., 2001; Wang et al., 2013) is excluded, as our reaction bottles were wrapped in Al-foil. Therefore, aqueous- and solid-phase As(V) in $As(III)_{spike}$ treatments is suggested to have formed via oxidation of surface-adsorbed As(III) by the Fe(II)-reacted Mgt or Mht, as has been previously reported for ferrihydrite (Zhang et al., 2019), goethite (Amstaetter et al., 2010), lepidocrocite (Wang and Giammar, 2015), and schwertmannite (Burton et al., 2010).

That As interactions with Fe(II)-reacted Mgt generally resulted in more changes in the As oxidation state and local coordination environment than with Mht may suggest that the presence of some structural Fe(II) aided the Fe(II)-catalyzed changes to As redox chemistry. Alternatively, as our study at pH 5.5 demonstrated, Fe(II) sorption onto Mgt was critical to enhancing As(V) removal from solution. Thus, it seems plausible that the efficiency of both As(III) oxidation and the structural incorporation of As(V) were similarly linked to the extent of Fe(II) uptake, which was higher in Mgt compared to Mht. This may also suggest that both As(III) oxidation and the structural incorporation of As(V) in systems comprising Fe(II) and non-stoichiometric magnetite or maghemite may be limited at lower pH, where Fe(II) sorption is inhibited. Similarly, the effects of Fe(II) sorption on As speciation and distribution are expected to decrease with stoichiometric magnetite, where Fe(II) uptake is limited. Because As(V) generally has a higher sorption affinity for Fe(III)-(oxyhydr)oxides (Dixit and Hering, 2003) and structurally incorporated As(V) is less easily desorbed (Huhmann et al., 2017; van Genuchten et al., 2020v), at circumneutral pH, non-stoichiometric magnetite and maghemite may represent significant pathways for long-term As sequestration at under reducing conditions, where Fe(II) is present.

CRediT authorship contribution statement

Reto Gubler: Investigation, Writing - original draft, Visualization. **Laurel K. ThomasArrigo:** Conceptualization, Investigation, Writing - review & editing, Visualization, Supervision, .

Declaration of Competing Interest

The authors declare that they have no known competing financial interests or personal relationships that could have appeared to influence the work reported in this paper.

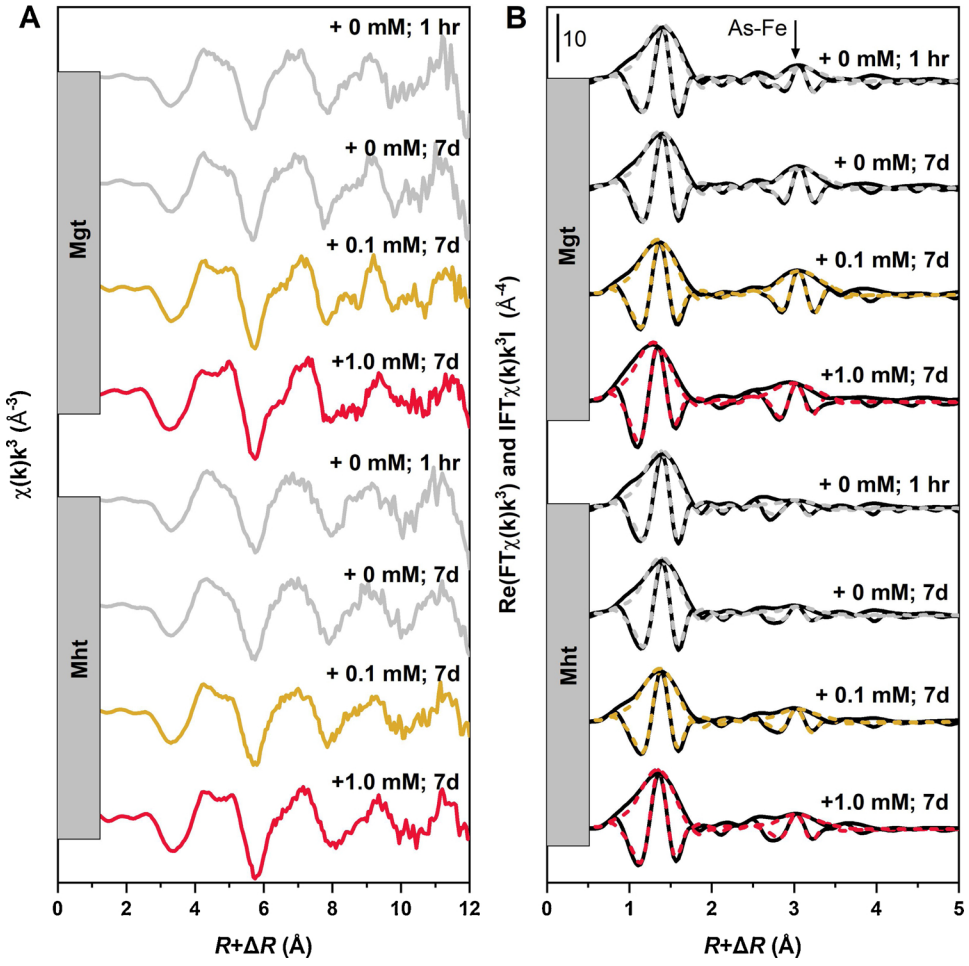

Fig. 5. (A) Arsenic K-edge EXAFS spectra and (B) Fourier-transform magnitudes and real parts shown for As(III)-spiked Mgt and Mht reacted with no additional Fe(II) (**gray**), 1.0 mM Fe(II) (**red**), and 0.1 mM Fe(II) (**yellow**). In (B), experimental data and model fits are shown in solid and dashed lines, respectively. Shell-fit parameters are reported in Table 1.

Table 1
Shell-fit parameters determined from As K-edge EXAFS spectra[a].

Sample	Treatment	Total As (mg/g)	As(V)[b] (%)	As-O			As-O-O[g]	As-Fe[h]		ΔE_0[i] (eV)	NSSR[j] (%)	red. χ^2[k]
				CN[c,d]	*R*[e] (Å)	σ^2[f] (Å²)	*R* (Å)	*CN*	*R* (Å)			
Mgt	+ As(V) (1 h)	0.69[l]	100	**4**	1.70(1)	0.002(1)	3.09(5)	1.3(6)	3.34(3)	8.5(17)	1.6	10
	+ As(V) (7 d)	0.98[m]	100	**4**	1.71(1)	0.002(1)	3.09(6)	1.5(8)	3.36(3)	8.9(19)	2.2	25
	+ As(III) (1 h)	0.85[l]	0	**3**	1.79(1)	0.003(1)	3.21(11)	2.0(5)	3.49(2)	12.6(8)	3.2	21
	+ As(III) (7 d)	1.2[m]	0	**3**	1.79(1)	0.003(1)	3.19(10)	3.1(5)	3.49(1)	10.9(16)	2.3	14
	+ 1.0 mM Fe(II) + As(V)	1.6[m]	100	**4**	1.70(1)	0.002(1)	3.08(3)	2.8(9)	3.42(3)	7.3(21)	2.4	60
	+ 1.0 mM Fe(II) + As(III)	1.5[m]	54	**3.54**	1.73(1)	0.004(1)	3.15(12)	2.9(6)	3.43(2)	7.2(24)	3.9	33
	+ 0.1 mM Fe(II) + As(V)	1.38[m]	100	**4**	1.70(1)	0.002(1)	3.10(7)	2.2(9)	3.39(2)	7.9(21)	2.3	41
	+ 0.1 mM Fe(II) + As(III)	1.20[m]	16	**3.16**	1.76(1)	0.003(1)	3.17(8)	3.7(4)	3.48(1)	11.1(7)	2.0	16
Mht	+ As(V) (1 h)	0.34[l]	100	**4**	1.71(1)	0.002(1)	3.06(5)	1.0(7)	3.32(5)	8.4(18)	2.0	15
	+ As(V) (7 d)	1.06[m]	100	**4**	1.70(1)	0.002(1)	3.09(6)	1.3(8)	3.33(4)	8.6(20)	2.3	35
	+ As(III) (1 h)	0.82[l]	0	**3**	1.79(1)	0.003(1)	3.19(12)	1.1(6)	3.42(3)	12.3(20)	4.1	22
	+ As(III) (7 d)	1.00[m]	0	**3**	1.79(1)	0.003(1)	3.19(10)	1.2(5)	3.46(3)	12.3(18)	3.0	16
	+ 1.0 mM Fe(II) + As(V)	1.72[m]	100	**4**	1.70(1)	0.002(1)	3.10(4)	1.3(9)	3.39(3)	8.8(20)	2.3	52
	+ 1.0 mM Fe(II) + As(III)	1.44[m]	29	**3.09**	1.75(1)	0.004(1)	3.16(11)	2.1(6)	3.45(2)	11.3(21)	3.9	42
	+ 0.1 mM Fe(II) + As(V)	1.43[m]	100	**4**	1.70(1)	0.002(1)	3.10(6)	1.4(8)	3.35(4)	8.7(19)	1.9	32
	+ 0.1 mM Fe(II) + As(III)	1.34[m]	9	**3.29**	1.78(1)	0.004(1)	3.18(11)	1.9(5)	3.45(2)	11.6(18)	3.0	22
Scorodite		357[m]	100	**4**	1.72(1)	0.001(1)	3.21(8)	**4**	3.38(2)	10.7(22)	2.6	84

[a]The passive amplitude reduction factor, S_0^2, was set to 1.0 for all experiment samples. Parameter uncertainties are shown for the last significant figure. Values in bold were fixed. [b]Fraction of As(V) determined by LCF analyses of As K-edge XANES spectra (Table S6). [c]Path degeneracy (coordination number). [d]Defined as: $N = 4f_{As(V)} + 3f_{As(III)}$. [e]Mean half path length. [f]Debye-Waller parameter. [g]Triangular multiple scattering path defined as: $CN = 12f_{As(V)} + 6f_{As(III)}$ and $\sigma^2 = 2\sigma^2_{As\text{-}O}$. [h]Debye-Waller parameter fixed to 0.008 or 0.0065 Å^2 for scorodite/As(V)$_{spike}$ and As(III)$_{spike}$ samples, respectively. [i]Energy-shift parameter. *j*Normalized sum of squared residuals; $= 100\Sigma_i(data_i\text{-}fit_i)^2/\Sigma_i data^2$. [k]Fit accuracy; $= (N_{idp}/N_{pts})\Sigma_i((data_i\text{-}fit_i)/\varepsilon_i)^2(N_{idp}\text{-}N_{var})^{-1}$. N_{idp}, N_{pts} and N_{var} are, respectively, the number of independent points in the model fit (16.3), the total number of data points, and the number of fit variables (6). ε_i is the uncertainty of the *i*th data point. [l]Calculated from [$As_{(aq)}$] assuming 100 % recovery (Tables S4 and S5). [m]Determined with ICP-OES after acid dissolution.

Acknowledgements

We are grateful to K. Barmettler, N. van Groeningen, S. Heller, M. Plötze, A. Röthlisberger, and M. Rothaupt (ETH Zurich) for assisting with laboratory analyses and R. Kretzschmar and J. M. Byrne for helpful discussions. We also thank the anonymous reviewers whose helpful comments improved the manuscript. We acknowledge APS, a User Facility of the U.S. Department of Energy Office of Science operated Argonne National Laboratory, contract No. DE-AC02-06CH11357 (APS) for the provision of synchrotron radiation facilities and we thank Q. Ma for support during the synchrotron measurements. This work was funded by ETH Zürich.

Appendix A. Supplementary data

Supplementary material related to this article can be found, in the online version, at doi:https://doi.org/10.1016/j.jhazmat.2020.123425.

References

Aeppli, M., Kaegi, R., Kretzschmar, R., Voegelin, A., Hofstetter, T.B., Sander, M., 2019. Electrochemical analysis of changes in iron oxide reducibility during abiotic ferrihydrite transformation into goethite and magnetite. Environ. Sci. Technol. 53, 3568–3578.

Amstaetter, K., Borch, T., Larese-Casanova, P., Kappler, A., 2010. Redox transformation of arsenic by Fe(II)- activated goethite (α-FeOOH). Environ. Sci. Technol. 44, 102–108.

Annersten, H., Hafner, S.S., 1973. Vacancy distribution in synthetic spinels of series Fe_3O_4 - $\gamma-Fe_2O_3$. Z. Kristallogr. 137, 321–340.

Bhandari, N., Reeder, R.J., Strongin, D.R., 2011. Photoinduced oxidation of arsenite to arsenate on ferrihydrite. Environ. Sci. Technol. 45, 2783–2789.

Bhandari, N., Reeder, R.J., Strongin, D.R., 2012. Photoinduced oxidation of arsenite to arsenate in the presence of goethite. Environ. Sci. Technol. 46, 8044–8051.

Burton, E.D., Johnston, S.G., Watling, K., Bush, R.T., Keene, A.F., Sullivan, L.A., 2010. Arsenic effects and behavior in association with the Fe(II)-catalyzed transformation of schwertmannite. Environ. Sci. Technol. 44, 2016–2021.

Burton, E.D., Johnston, S.G., Bush, R.T., 2011. Microbial sulfidogenesis in ferrihydrite-rich environments: effects on iron mineralogy and arsenic mobility. Geochim. Cosmochim. Acta 75, 3072–3087.

Burton, E.D., Johnston, S.G., Planer-Friedrich, B., 2013. Coupling of arsenic mobility to sulfur transformations during microbial sulfate reduction in the presence and absence of humic acid. Chem. Geol. 343, 12–24.

Burton, E.D., Hockmann, K., Karimian, N., 2020. Antimony sorption to goethite: effects of Fe(II)-catalyzed recrystallization. ASC Earth Space Chem. 4, 476–487.

Catalano, J.G., Luo, Y.M., Otemuyiwa, B., 2011. Effect of aqueous Fe(II) on arsenate sorption on goethite and hematite. Environ. Sci. Tech. 45, 8826–8833.

Chaudhuri, S.K., Lack, J.G., Coates, J.D., 2001. Biogenic magnetite formation through anaerobic biooxidation of Fe(II). Appl. Environ. Microb. 67, 2844–2848.

Chowdhury, S.R., Yanful, E.K., Pratt, A.R., 2011. Arsenic removal from aqueous solutions by mixed magnetite- maghemite nanoparticles. Environ. Earth Sci. 64, 411–423.

Coker, V.S., Gault, A.G., Pearce, C.I., van der Laan, G., Telling, N.D., Charnock, J.M., Polya, D.A., Lloyd, J.R., 2006. XAS and XMCD evidence for species-dependent partitioning of arsenic during microbial reduction of ferrihydrite to magnetite. Environ. Sci. Technol. 40, 7745–7750.

Cornell, R.M., Schwertmann, U., 2003. The Iron Oxides: Structure, Properties, Reactions, Occurances and Uses. Wiley-VCH, Weinheim, Germany.

Cummings, D.E., Caccavo, F., Fendorf, S., Rosenzweig, R.F., 1999. Arsenic mobilization by the dissimilatory Fe(III)-reducing bacterium *Shewanella alga* BrY. Environ. Sci. Technol. 33, 723–729.

Dixit, S., Hering, J.G., 2003. Comparison of arsenic(V) and arsenic(III) sorption onto iron oxide minerals: implications for arsenic mobility. Environ. Sci. Technol. 37, 4182–4189.

Dixit, S., Hering, J.G., 2006. Sorption of Fe(II) and As(III) on goethite in single- and dual-sorbate systems. Chem. Geol. 228, 6–15.

Ehlert, K., Mikutta, C., Jin, Y., Kretzschmar, R., 2018. Mineralogical controls on the bioaccessibility of arsenic in Fe(III)-As(V) coprecipitates. Environ. Sci. Technol. 52, 616–627.

Farquhar, M.L., Charnock, J.M., Livens, F.R., Vaughan, D.J., 2002. Mechanisms of arsenic uptake from aqueous solution by interaction with goethite, lepidocrocite, mackinawite, and pyrite: an X-ray absorption spectroscopy study. Environ. Sci. Technol. 36, 1757–1762.

Fleet, M.E., 1981. The structure of magnetite. Acta Crystallogr. B 37, 917–920.

Fortune, W.B., Mellon, M.G., 1938. Determination of iron with *o*-phenanthroline - A spectrophotometric study. Ind. Eng. Chem., Anal. Ed. 10, 60–64.

Frierdich, A.J., Catalano, J.G., 2012a. Controls on Fe(II)-activated trace element release from goethite and hematite. Environ. Sci. Technol. 46, 1519–1526.

Frierdich, A.J., Catalano, J.G., 2012b. Fe(II)-mediated reduction and repartitioning of structurally incorporated Cu, Co, and Mn in iron oxides. Environ. Sci. Technol. 46, 11070–11077.

Frierdich, A.J., Helgeson, M., Liu, C., Wang, C., Rosso, K.M., Scherer, M.M., 2015. Iron atom exchange between hematite and aqueous Fe(II). Environ. Sci. Technol. 49, 8479–8486.

Gorski, C.A., Scherer, M.M., 2009. Influence of magnetite stoichiometry on Fe^{II} uptake and nitrobenzene reduction. Environ. Sci. Tech. 43, 3675–3680.

Gorski, C.A., Scherer, M.M., 2010. Determination of nanoparticulate magnetite stoichiometry by Mössbauer spectroscopy, acidic dissolution, and powder X-ray diffraction: a critical review. Am. Miner. 95, 1017–1026.

Gorski, C.A., Handler, R.M., Beard, B.L., Pasakarnis, T., Johnson, C.M., Scherer, M.M., 2012. Fe atom exchange between aqueous Fe^{2+} and magnetite. Environ. Sci. Technol. 46, 12399–12407.

Gotić, M., Koščec, G., Musić, S., 2009. Study of the reduction and reoxidation of substoichiometric magnetite. J. Mol. Struct. 924, 347–354.

Greaves, C., 1983. A powder neutron diffraction investigation of vacancy ordering and covalence in γ-Fe_2O_3. J. Solid State Chem. 49, 325–333.

Handler, R.M., Frierdich, A.J., Johnson, C.M., Rosso, K.M., Beard, B.L., Wang, C., Latta, D.E., Neumann, A., Pasakarnis, T., Premaratne, W.A.P.J., Scherer, M.M., 2014. Fe(II)-catalyzed recrystallization of goethite revisited. Environ. Sci. Technol. 48, 11302–11311.

Hansel, C.M., Benner, S.G., Neiss, J., Dohnalkova, A., Kukkadapu, R.K., Fendorf, S., 2003. Secondary mineralization pathways induced by dissimilatory iron reduction of ferrihydrite under advective flow. Geochim. Cosmochim. Acta 67, 2977–2992.

Hiemstra, T., van Riemsdijk, W.H., 2007. Adsorption and surface oxidation of Fe(II) on metal (hydr)oxides. Geochim. Cosmochim. Acta 71, 5913–5933.

Hug, S.J., Leupin, O., 2003. Iron-catalyzed oxidation of arsenic(III) by oxygen and by hydrogen peroxide: pH- dependent formation of oxidants in the Fenton reaction. Environ. Sci. Technol. 37, 2734–2742.

Hug, S.J., Canonica, L., Wegelin, M., Gechter, D., Von Gunten, U., 2001. Solar oxidation and removal of arsenic at circumneutral pH in iron containing waters. Environ. Sci. Technol. 35, 2114–2121.

Huhmann, B.L., Neumann, A., Boyanov, M.I., Kemner, K.M., Scherer, M.M., 2017. Emerging investigator series: As(v) in magnetite: incorporation and redistribution. Env. Sci.-Proc. Imp. 19, 1208–1219.

IUPAC, 2005. Nomenclature of inorganic chemistry. IUPAC Recommendations in.

Jang, J.H., Dempsey, B.A., 2008. Coadsorption of arsenic(III) and arsenic(V) onto hydrous ferric oxide: effects on abiotic oxidation of arsenic(III), extraction efficiency, and model accuracy. Environ. Sci. Technol. 42, 2893–2898.

Jiang, S., Lee, J.H., Kim, D., Kanaly, R.A., Kim, M.G., Hur, H.G., 2013. Differential arsenic mobilization from As- bearing ferrihydrite by iron-respiring *Shewanella* strains with different arsenic-reducing activities. Environ. Sci. Technol. 47, 8616–8623.

Jolivet, J.P., Belleville, P., Tronc, E., Livage, J., 1992. Influence of Fe(II) on the formation of the spinel iron oxide in alkaline medium. Clay. Clay Miner. 40, 531–539.

Jönsson, J., Sherman, D.M., 2008. Sorption of As(III) and As(V) to siderite, green rust (fougerite) and magnetite: implications for arsenic release in anoxic groundwaters. Chem. Geol. 255, 173–181.

Kim, M.J., Nriagu, J., 2000. Oxidation of arsenite in groundwater using ozone and oxygen. Sci. Total Environ. 247, 71–79.

Kocar, B.D., Borch, T., Fendorf, S., 2010. Arsenic repartitioning during biogenic sulfidization and transformation of ferrihydrite. Geochim. Cosmochim. Acta 74, 980–994.

Langmuir, D., Mahoney, J., Rowson, J., 2006. Solubility products of amorphous ferric arsenate and crystalline scorodite ($FeAsO_4 \cdot 2H_2O$) and their application to arsenic behavior in buried mine tailings. Geochim. Cosmochim. Acta 70, 2942–2956.

Latta, D.E., Gorski, C.A., Boyanov, M.I., O'Loughlin, E.J., Kemner, K.M., Scherer, M.M., 2012. Influence of magnetite stoichiometry on U^{VI} reduction. Environ. Sci. Technol. 46, 778–786.

Liu, C.H., Chuang, Y.H., Chen, T.Y., Tian, Y., Li, H., Wang, M.K., Zhang, W., 2015. Mechanism of arsenic adsorption on magnetite nanoparticles from water: thermodynamic and spectroscopic studies. Environ. Sci. Technol. 49, 7726–7734.

Lovley, D.R., Stolz, J.F., Nord, G.L., Phillips, E.J.P., 1987. Anaerobic production of magnetite by a dissimilatory iron-reducing microorganism. Nature 330, 252–254.

Mikutta, C., Frommer, J., Voegelin, A., Kaegi, R., Kretzschmar, R., 2010. Effect of citrate on the local Fe coordination in ferrihydrite, arsenate binding, and ternary arsenate complex formation. Geochim. Cosmochim. Acta 74, 5574–5592.

Morin, G., Rousse, G., Elkaim, E., 2007. Crystal structure of tooeleite, $Fe_6(AsO_3)_4SO_4(OH)_4 \cdot 4H_2O$, a new iron arsenite oxyhydroxysulfate mineral relevant to acid mine drainage. Am. Miner. 92, 193–197.

Morin, G., Ona-Nguema, G., Wang, Y., Menguy, N., Juillot, F., Proux, O., Guyot, F., Calas, G., Brown, G.E., 2008. Extended X-ray absorption fine structure analysis of arsenite and arsenate adsorption on maghemite. Environ. Sci. Technol. 42, 2361–2366.

Morin, G., Wang, Y.H., Ona-Nguema, G., Juillot, F., Calas, G., Menguy, N., Aubry, E., Bargar, J.R., Brown, G.E., 2009. EXAFS and HRTEM evidence for As(III)-containing surface precipitates on nanocrystalline magnetite: implications for As sequestration. Langmuir 25, 9119–9128.

Muehe, E.M., Scheer, L., Daus, B., Kappler, A., 2013. Fate of arsenic during microbial reduction of biogenic versus abiogenic As-Fe(III)-mineral coprecipitates. Environ. Sci. Technol. 47, 8297–8307.

Ona-Nguema, G., Morin, G., Wang, Y., Foster, A.L., Juillot, F., Calas, G., Brown, G.E., 2010. XANES evidence for rapid arsenic(III) oxidation at magnetite and ferrihydrite surfaces by dissolved O_2 via Fe^{2+}- mediated reactions. Environ. Sci. Technol. 44, 5416–5422.

Oscarson, D.W., Huang, P.M., Liaw, W.K., 1980. The oxidation of arsenite by aquatic sediments. J. Environ. Qual. 9, 700–703.

Pasakarnis, T.S., Boyanov, M.I., Kemner, K.M., Mishra, B., O'Loughlin, E.J., Parkin, G., Scherer, M.M., 2013. Influence of chloride and Fe(II) content on the reduction of Hg (II) by magnetite. Environ. Sci. Technol. 47, 6987–6994.

Pedersen, H.D., Postma, D., Jakobsen, R., 2006. Release of arsenic associated with the reduction and transformation of iron oxides. Geochim. Cosmochim. Acta 70, 4116–4129.

Perez, J.P.H., Tobler, D.J., Thomas, A.N., Freeman, H.M., Dideriksen, K., Radnik, J., Benning, L.G., 2019. Adsorption and reduction of arsenate during the Fe^{2+}-induced transformation of ferrihydrite. ACS Earth Space Chem. 3, 884–894.
Ravel, B., Newville, M., 2005. ATHENA, ARTEMIS, HEPHAESTUS: data analysis for X-ray absorption spectroscopy using IFEFFIT. J. Synchrotron Radiat. 12, 537–541.
Reddy, T.R., Frierdich, A.J., Beard, B.L., Johnson, C.M., 2015. The effect of pH on stable iron isotope exchange and fractionation between aqueous Fe(II) and goethite. Chem. Geol. 397, 118–127.
Roberts, L.C., Hug, S.J., Ruettimann, T., Billah, M., Khan, A.W., Rahman, M.T., 2004. Arsenic removal with iron(II) and iron(III) waters with high silicate and phosphate concentrations. Environ. Sci. Tech. 38, 307–315.
Sheng, A.X., Liu, J., Li, X.X., Qafoku, O., Collins, R.N., Jones, A.M., Pearce, C.I., Wang, C., Ni, J.R., Lu, A.H., Rosso, K.M., 2020. Labile Fe(III) from sorbed Fe(II) oxidation is the key intermediate in Fe(II)- catalyzed ferrihydrite transformation. Geochim. Cosmochim. Acta 272, 105–120.
Sidhu, P.S., Gilkes, R.J., Cornell, R.M., Posner, A.M., Quirk, J.P., 1981. Dissolution of iron-oxides and oxyhydroxides in hydrochloric and perchloric acids. Clay. Clay Miner. 29, 269–276.
Smedley, P.L., Kinniburgh, D.G., 2002. A review of the source, behaviour and distribution of arsenic in natural waters. Appl. Geochem. 17, 517–568.
Sundman, A., Vitzthum, A.L., Adaktylos-Surber, K., Figueroa, A.I., van der Laan, G., Daus, B., Kappler, A., Byrne, J.M., 2020. Effect of Fe-metabolizing bacteria and humic substances on magnetite nanoparticle reactivity towards arsenic and chromium, J. Haz. Mat. 384.
Tamaura, Y., Ito, K., Katsura, T., 1983. Transformation of γ-FeO(OH) to Fe_3O_4 by adsorption of iron(II) ion on γ- FeO(OH). J. Chem. Soc. Dalton 189–194.
ThomasArrigo, L.K., Mikutta, C., Lohmayer, R., Planer-Friedrich, B., Kretzschmar, R., 2016. Sulfidization of organic freshwater flocs from a minerotrophic peatland: speciation changes of iron, sulfur, and arsenic. Environ. Sci. Technol. 50, 3607–3616.
Tronc, E., Jolivet, J.P., Lefebvre, J., Massart, R., 1984. Ion adsorption and electron transfer in spinel-like iron oxide colloids. J. Chem. Soc. Farad. T. 1 (80), 2619–802629.
van Genuchten, C.M., Behrends, T., Stipp, S.L.S., Dideriksen, K., 2020v. Achieving arsenic concentrations of < 1 μg/L by Fe(0) electrolysis: The exceptional performance of magnetite. Water Res. 168.
Voegelin, A., Weber, F.A., Kretzschmar, R., 2007. Distribution and speciation of arsenic around roots in a contaminated riparian floodplain soil: Micro-XRF element mapping and EXAFS spectroscopy. Geochim. Cosmochim. Acta 71, 5804–5820.
Wang, L., Giammar, D., 2015. Effects of pH, dissolved oxygen, and aqueous ferrous iron on the adsorption of arsenic to lepidocrocite. J. Colloid Interf. Sci. 448, 331–338.
Wang, Y., Morin, G., Ona-Nguema, G., Menguy, N., Juillot, F., Aubry, E., Guyot, F., Calas, G., Brown Jr., G.E., 2008. Arsenite sorption at the magnetite-water interface during aqueous precipitation of magnetite: EXAFS evidence for a new arsenite surface complex. Geochim. Cosmochim. Acta 72, 2573–2586.
Wang, Y.H., Morin, G., Ona-Nguema, G., Juillot, F., Calas, G., Brown, G.E., 2011. Distinctive arsenic(V) trapping modes by magnetite nanoparticles induced by different sorption processes. Environ. Sci. Tech. 45, 7258–7266.
Wang, Y.J., Xu, J., Zhao, Y., Zhang, L., Xiao, M., Wu, F., 2013. Photooxidation of arsenite by natural goethite in suspended solution. Environ. Sci. Pollut. R. 20, 31–38.
Wang, Y.H., Morin, G., Ona-Nguema, G., Brown, G.E., 2014. Arsenic(III) and arsenic(V) speciation during transformation of lepidocrocite to magnetite. Environ. Sci. Technol. 48, 14282–14290.
WHO, 2011. Guidelines for Drinking-water Quality. World Health Organization, Geneva.
Xu, Y., Zhou, G.-P., Zheng, X.-F., 2007. Redetermination of iron(III) arsenate dihydrate. Acta Crystallogr. E 63, i67–i69.
Yean, S., Cong, L., Yavuz, C.T., Mayo, J.T., Yu, W.W., Kan, A.T., Colvin, V.L., Tomson, M.B., 2005. Effect of magnetite particle size on adsorption and desorption of arsenite and arsenate. J. Mater. Res. 20, 3255–3264.
Zabinsky, S.I., Rehr, J.J., Ankudinov, A., Albers, R.C., Eller, M.J., 1995. Multiple-scattering calculations of X-ray absorption spectra. Phys. Rev. B 52, 2995–3009.
Zhang, G.Q., Yuan, Z.D., Lei, L., Lin, J.R., Wang, X., Wang, S.F., Jia, Y.F., 2019. Arsenic redistribution and transformation during Fe(II)-catalyzed recrystallization of As-adsorbed ferrihydrite under anaerobic conditions. Chem. Geol. 525, 380–389.